Journal of Applied Polymer Science

Dynamic rheological behavior of reactively compatibilized polypropylene/polyamide 6 blending melts

Hua-yong Liao, Lu-yao Zheng, Yong-bing Hu, Xian-jun Zha, Xiang Xu, Yan-wei Wen, Guo-liang Tao, Chun-lin Liu

School of Materials Science and Engineering, Changzhou University, Changzhou 213164, China

Correspondence to: H.-y. Liao (E-mail: roynetlhy@163.com)

ABSTRACT: The dynamic rheological behavior is measured by small amplitude oscillatory shear on rotational rheometer for polypropylene/polyamide 6 (PP/PA6) blends compatibilized by a polypropylene grafted maleic anhydride (PP-*g*-MAH). Scanning electron microscope (SEM) results show that the PP/PP-*g*-MAH/PA6 (=100/6/40wt) is sea-island structure, the PP/PP-*g*-MAH/PA6 (=100/6/60wt) blend is semi-cocontinuous. Coarse PA6 zones can be observed when the weight ratio is 100/6/80. At low frequency the complex viscosity, dynamic modulus of the PP/PP-*g*-MAH/PA6 (PP/PP-*g*-MAH = 100/6wt) blends first increase then drop with the increase of PA6 weight content in the range of 0–100, the maximum value arrives at the weight content of 60. The Cole–Cole plots as well as the weighted relaxation spectra of the blends have a main arc and a tail when the weight ratio of PP/PP-*g*-MAH/PA6 is in the range of 100/6/20–100/6/60, but have different shapes when the weight ratio increases to 100/6/80 and 100/6/100. The possible reason is the weight ratio of 100/6/80 and 100/6/100 is close to the phase inversion point. In fitting the storage modulus data at low frequency, Palierne's model with two parameters interfacial tension and interfacial shear modulus is better than Bousmina's model. Palierne's model with only one parameter of interfacial tension can not fit the data well. © 2015 Wiley Periodicals, Inc. J. Appl. Polym. Sci. **2015**, *132*, 42091.

KEYWORDS: blends; compatibilization; phase behavior; polyamides; rheology

Received 17 October 2014; accepted 9 February 2015

DOI: 10.1002/app.42091

INTRODUCTION

Polypropylene (PP) is a versatile polymer with good mechanical properties besides its low costs, such as chemical and thermal resistance, etc., but with relatively poor solvent barrier properties. While polyamide 6 (PA6) has its special properties such as solvent barrier properties, good flowability, low friction, and so on. Blending PP and PA6 with proper compatibilizer enables PP/PA6 alloy with desirable properties to be developed.[1]

The mechanical properties,[2–4] thermal and heat oxidation[5] of PP/PA6 blends were investigated. It is well known that the properties of polymer blends are closely related to their phase morphology. Rheological especially dynamic rheological behavior of polymer blends has been paid much attention since dynamic rheological measurement with small amplitude oscillatory mode is sensitive to the microstructure of polymer blends.[6] Some classic emulsion models can relate the rheological behavior to the interfacial tension between the blending components, such as Palierne's model[7] as well as Choi and Schowalter's model.[8] The former can describe the linear viscoelastic response of polymer blends under some assumptions, for example, the distribution of the dispersed droplets is relatively narrow, the shape of the droplet is spherical. The latter is suitable to dilute and semi-dilute regimes in predicting rheological behavior. Based on the Choi and Schowalter's model a constitutive equation for an emulsion was introduced by Gramespacher and Meissner.[9]

Some researches have been done on the rheological behavior and interface tension for PP/PA6 blends.[10] Similar works are available about two polymer blends PS/PMMA and PDMS/POE-DO.[11] For immiscible PP/PA6 blends there are two different morphologies, i.e., droplet-matrix structure and cocontinuous structure, and phase inversion may happen at some component weight ratio or some temperature. The HDPE/PA6 (=50/50 wt) blends can reveal sea-island structure, cocontinuous structure and phase inversion, respectively, when a certain amount of functionalized multiwalled carbon nanotubes (FMWCNTs) are added into the blends.[12] Generally in this case the abovementioned emulsion models can not work well.

Relaxation is an important characteristic for polymer systems, which have entangled long chains and can disentangle or orientate when being sheared or stretched. The relaxation mechanism of heterogeneous polymers can be obviously displayed by Cole–Cole diagram.[13] Generally two circle arcs can be observed for

polymer blends, which means the happening of two simultaneous processes with different relaxation times for the two different phases, respectively. This kind of work is available, such as the Cole–Cole plots for PA6/HDPE =85/15 (wt) blends and PA6/EPDM-*g*-MA = 85/15 (wt) blends.[14]

The relaxation process of polymer blends can be more clearly indicated by relaxation time spectrum. Various models can be applied to obtain relaxation time spectrum by fitting the relaxation modulus or dynamic modulus data, such as generalized Maxwell model,[15] Tschoegle approximation model,[16] and so on. The relaxation of the dispersed droplets mainly shows at low frequency for small amplitude oscillatory shear (SAOS). The weighted relaxation spectrum of PP/PS (90/10) blends was calculated by Macaúbas and Demarquette.[17]

In this work, the dynamic rheological behavior of PP/PA6 blending melts compatibilized with a polypropylene grafted maleic anhydride (PP-*g*-MAH) is investigated. Different emulsion models have been applied to fit the storage moduli data. The Cole–Cole plots, relaxation time spectrum of the blends are discussed.

EXPERIMENTAL

Materials

PP T30S is produced by Dalian Petro, China. Its melt flow rate (MFR) is 3.5 g (10 min)$^{-1}$, measured at 230°C, 2.16 kg. Its mass average and number-average molar masses are Mw = 263,000 g mol^{-1} and Mn= 38,000 g mol^{-1}, respectively. PA6 1013B produced in Japan Ube has a MFR = 45 g (10 min)$^{-1}$, measured at 250°C, 2.16 kg. The number-average molar mass of PA6 is 26,000 g mol^{-1}. PP-*g*-MAH is homemade with a grafting rate of 1.0%. Its mass average and number-average molar masses are Mw = 61,200 g mol^{-1} and Mn = 33,000 g mol^{-1}, respectively. Its melt flow rate (MFR) is 16.2 g (10 min)$^{-1}$, measured at 230°C, 2.16 kg.

Preparation of PP-*g*-MAH and Blends

To prepare the PP-*g*-MAH, 1000 g pure PP particles were first mixed with 10 mL liquid paraffin, then 1.5 g antioxidant 1010, 1 g dicumyl peroxide (DCP) and 3 g maleic anhydride (MAH) were added in, and all the components were mixed by using a high-speed mixer (produced by Fuxin Light Industry Machinery Factory) for 2 min, then the mixed samples were fed into a corotating twin screw extruder (type SHJ-35, made in Rubber and Plastic Machinery Factory), melt, and extruded through a die, then were cooled under water, granulated by a granulator, and were dried at 120°C for 12 h in an electric blast drying oven. The rotating speed of the screw extruder was 110 r min^{-1}, the feeding speed was 100 r min^{-1}, and the temperature of the nine zones of the barrel was 150, 175, 180, 200, and 210°C (the same temperature from the fifth to the ninth zone), the temperature of the die was 210°C.

The materials were dried at 85°C for 12 h in an electric blast drying oven, then were mixed in a high-speed mixer with the weight ratio PP/PP-*g*-MAH/PA6 of 100/6/0, 100/6/20, 100/6/40, 100/6/60, 100/6/80, and 100/6/100. After that the samples were fed into a corotating twin screw extruder, melt and extruded through a die, then were cooled under water, granulated by a granulator, and were dried at 120°C for 12 h in an electric blast drying oven. The rotating speed of the screw extruder was 110 r min^{-1}, the feeding speed was 100 r min^{-1}, and the temperature of the nine zones of the barrel was 150, 175,180, 200, 210, and 230°C (the same temperature from the sixth to the ninth zone), the temperature of the die was 230°C.

Measurement of Performances

Scanning electron microscope (SEM): the PP/PP-*g*-MAH/PA6 samples were thrust at an Izod impact test machine ADN-5.5 produced by Heng Shang Industrial Equipment Factory. Then the fractured surface was etched by 98% formic acid solution at 50°C for 3 min to extract the PA6 phase. Afterwards the cross section was washed repeatedly by deionized water, then was dried in an electric blast drying oven at 110°C for 12 h. The cross section was sprayed with gold and was observed by SEM LE0438VP made by Hitachi Company, Japan, at an accelerating voltage of 15 kV.

Rheological measurement: All the samples for rheological measurement were prepared by using compression molding at 240°C and at pressure of 10 MPa for 5 min. The heated samples were then compressed at room temperature at 10 MPa for 3 min. The diameter and thickness of samples were 25 and 2 mm, respectively. Small amplitude oscillatory shear(SAOS) was applied by using a rotational rheometer MCR301 made by Anton Paar Gmb of Austria with two parallel plates. The diameter of the plate is 25 mm, the gap of the two plates is 1 mm. The surplus compressed by the top plate were trimmed carefully. The temperature in the rheological measurement was 230°C, and the angular frequency was from 0.028 to 300 rad s^{-1} in an ascending order and at strain amplitude of 4% which was within the linear viscoelastic region. The linear viscoelastic regime was determined by applying strain sweeping. The measurement was under nitrogen atmosphere to avoid the oxidization of the samples. Before the start of the measurement the samples were kept for 5 min between the gap of the two plates to eliminate thermal history.

RESULTS AND DISCUSSION

SEM Micrographs of PP/PP-*g*-MAH/PA6 Blends

Figure 1(a,c,d) shows the morphologies of PP/PA6 blends compatibilized by PP-*g*-MAH with PA6 content 40, 60 and 80, respectively by the same magnification times (×1000). Figure 1(b) is PP/PP-*g*-MAH/PA6 = 100/6/40 with magnification times (×3000). Figure 1(a) shows the dispersed PA6 droplets in the PP matrix. The average radius of the dispersed PA6 droplet is 0.25 μm. Figure 1(c) shows the coarse phases of the blend, there are both dispersed PA6 droplets and semi-cocontinuous phases. Figure 1(d) shows the morphology of PP/PP-*g*-MAH/PA6 = 100/6/80 blend. Also both dispersed droplets and large continuous phase zone exist [see the marked circles in the Figure 1(d)], the phase size of the droplet is very nonuniform, the large radius is more than 12 μm, while the small droplet radius is about 1 μm. The morphology of PP/PP-*g*-MAH/PA6 = 100/6/100 blend is not shown, the weight ratio is close to phase inversion.[2]

Dynamic Rheological Curves of PP/PP-*g*-MAH/PA6 Blending Melts

Figure 2 shows the complex viscosity of the PP/PP-*g*-MAH/PA6 (PP/PP-*g*-MAH = 100/6)blends and their pure components. As the weight content of PA6 increases, the complex viscosity of

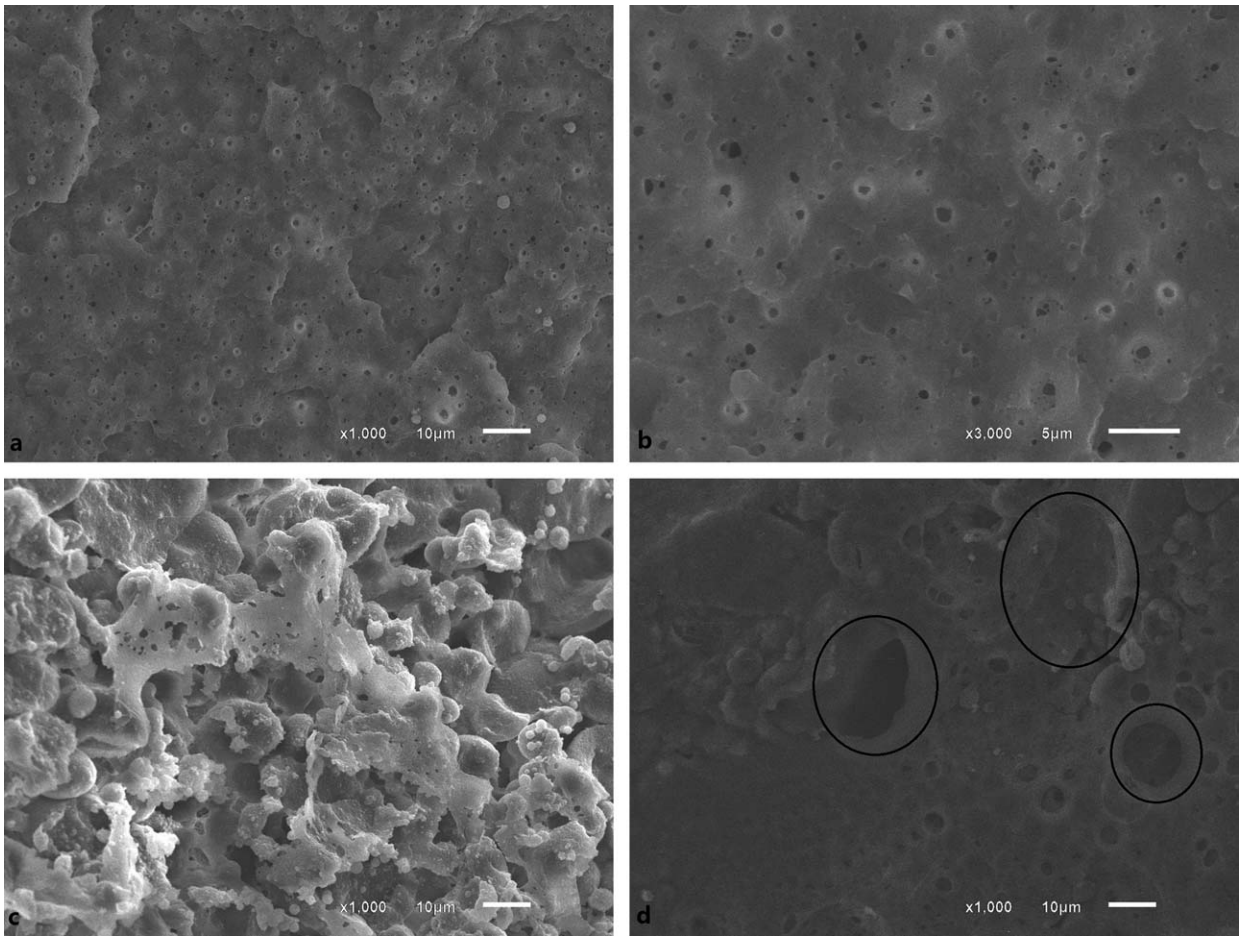

Figure 1. SEM photo of (a) PP/PP-*g*-MAH/PA6 = 100/6/40 (×1000), (b) PP/PP-*g*-MAH/PA6 = 100/6/40 (×3000), (c) PP/PP-*g*-MAH/PA6 = 100/6/60 (×1000), (d) PP/PP-*g*-MAH/PA6 = 100/6/80 blends (×1000).

the blends at low frequency increases, and the viscosity value arrives the highest at PA6 weight content of 60. Remembering the SEM microstructure shown in Figure 1(c), the semi-cocontinuous phase structure of PA6 with content of 60 results from the fine compatibilization between PP and PA6 by PP/PP-*g*-MAH, which supports the relatively high complex viscosity at low frequency. Then, the complex viscosity drops when the weight content continues to increase from 80 to 100. The measured zero shear viscosity of pure PA6 at 230°C is 388 Pa s, much lower than that of PP/PP-*g*-MAH = 100/6(wt) blend, i.e. 3630 Pa s, thus high viscosity phase (PP) is packed by low viscosity phase (PA6), which leads to falling of the viscosity of the blend after phase inversion point (PP/PA6 = 50/50).[2]

The storage modulus and loss modulus had the same trend as the complex viscosity, as shown in Figure 3. At high frequency, the storage as well as loss modulus curves of different weight content of PA6 overlapped. The rheological behavior at low frequency is related to the morphology of the blend. The storage modulus at low frequency is more sensitive to the relaxation of the dispersed droplets than the loss modulus. The interfacial tension between PP and PA6 is 13.61 mN m^{-1} at 230°C.[18] It is reported that the addition of PP-*g*-MAH decreases the interfacial tension between PA6 and PP obviously.[10]

Figure 4 shows the Cole–Cole plot (η" versus η') of the blends and the pure components. The Cole–Cole plot can generally display two frequency regimes in multiphase polymer blends, corresponding to different relaxation mechanisms.[14] It can be seen from Figure 4 that the pure PA6 and PP has only one relaxation arc. This is the case, because they are homogeneous

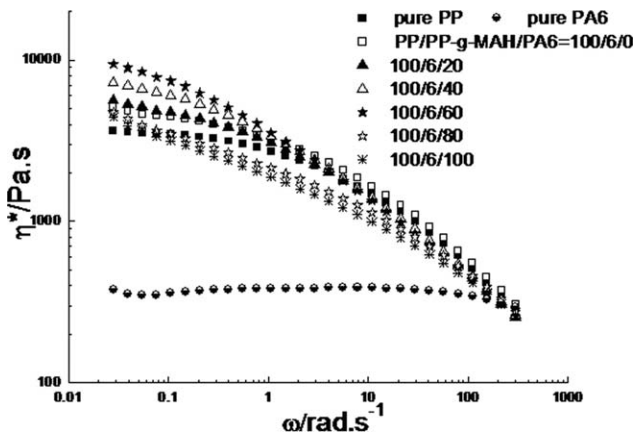

Figure 2. Complex viscosity vs. angular frequency of PP/PP-*g*-MAH/PA6 blends and pure PP and PA6 at 230°C.

polymer melts. For the blends, the Cole–Cole plot shows one main arc and a tail, the arc corresponds to the relaxation of the matrix, i.e., the PP phase, and the tail corresponds to the relaxation of PA6, the dispersed phase. As the PA6 weight content increases from 0 to 60, the radius of the main arc increases, which means the relaxation time increases. The Cole–Cole plots of the blend with PA6 weight content 80 and 100 are different from those below weight content 80, the tails are straight upward and the relaxation spectra are relatively lower. This is possibly due to phase inversion happens when PA6 weight content is close to 100, thus the dispersed PP phase spreads over the matrix phase PA6. The pure PA6 has the smallest main arc, since its relaxation time is shortest compared to that of the blend.

Interfacial Tension of PP/PP-*g*-MAH/PA6 Blending Melts

The Palierne's model can describe the viscoelastic behavior of the incompressible nondilute emulsions. The complex shear modulus of the blend is expressed as[7,19]

$$G* = G*_m\left[\frac{1+\frac{3}{2}\sum_i \frac{\emptyset E_i}{D_i}}{1-\sum_i \frac{\emptyset E_i}{D_i}}\right] \quad (1)$$

where

$$E_i = 2(G^*_d - G^*_m)(19G^*_d + 16G^*_m) + \frac{48\beta^*_d\alpha}{R_i^2} + \frac{32\beta^*_s(\alpha+\beta^*_d)}{R_i^2} + \frac{8\alpha}{R_i}(5G^*_d + 2G^*_m) + \frac{2\beta^*_d}{R_i}(23G^*_d - 16G^*_m) + \frac{4\beta^*_s}{R_i}(13G^*_d + 8G^*_m) \quad (2)$$

and

$$D_i = (2G^*_d + 3G^*_m)(19G^*_d + 16G^*_m) + \frac{48\beta^*_d\alpha}{R_i^2} + \frac{32\beta^*_s(\alpha+\beta^*_d)}{R_i^2} + \frac{40\alpha}{R_i}(G^*_d + G^*_m) + \frac{2\beta^*_d}{R_i}(23G^*_d + 32G^*_m) + \frac{4\beta^*_s}{R_i}(13G^*_d + 12G^*_m) \quad (3)$$

The subscript "*i*" refers to the *i*th particle fraction,Ø is the volume fraction of the dispersed phase. *R* is the dispersed particle radius. G^*_d and G^*_m is the complex modulus of the dispersed phase and matrix, respectively. The interfacial tension effect described by this model consists of two aspects, one is the equilibrium interfacial tension α, another is the complex moduli $\beta^*(\omega)$. $\beta^*(\omega)$ consists of two complex moduli: surface dilatation modulus $\beta^*_d(\omega)$ and surface shear modulus $\beta^*_s(\omega)$. The surface dilatation modulus $\beta^*_d(\omega)$ is related to interfacial area variation, and the surface shear modulus $\beta^*_s(\omega)$ is associated with the resistance of the interface to the shear deformation. In the linear viscoelastic regime, the deformation of dispersed phase is small and the values of the complex modulus $\beta^*_d(\omega)$ and $\beta^*_s(\omega)$ can be assumed to be zero, thus the simplified form of Palierne's model can be expressed as eq. (4).

$$G*(\omega) = G*_m(\omega)\left[\frac{1+3\sum_i \emptyset_i H_i(\omega)}{1-2\sum_i \emptyset_i H_i(\omega)}\right] \quad (4)$$

where

$$H(\omega) = \frac{4(\alpha/R)[2G^*_m(\omega)+5G^*_d(\omega)] + [G^*_d(\omega)-G^*_m(\omega)][16G^*_m(\omega)+19G^*_d(\omega)]}{40(\alpha/R)[G^*_m(\omega)+G^*_d(\omega)] + [2G^*_d(\omega)+3G^*_m(\omega)][16G^*_m(\omega)+19G^*_d(\omega)]} \quad (5)$$

Similar to Palierne's model, Bousmina's model[20] gives the complex shear modulus of the blend as a function of the same parameter by

$$G^*(\omega) = G^*_m(\omega) \times \frac{2(G^*_d(\omega)+\alpha/R) + 3G^*_m(\omega) + 3\emptyset[G^*_d(\omega)+\alpha/R-G^*_m(\omega)]}{2(G^*_d(\omega)+\alpha/R) + 3G^*_m(\omega) - 2\emptyset[G^*_d(\omega)+\alpha/R-G^*_m(\omega)]} \quad (6)$$

It is reported[20,21] that the Palierne's model and Bousmina's model give similar predicting results for usual polymer blends, furthermore, the difference between the two models is the latter accounts for structured drops such as LCPs.

Figure 5 shows the storage modulus versus frequency ($G' \sim \omega$) data fit by Palierne's model with only one parameter α/R, i.e., eq. (4). The fitting was done at limited low frequency range, i.e., 0.028–1.07 rad s^{-1}, because the interfacial tension is sensitive to low frequency, and insensitive to high frequency. It can be found that the fitting is not satisfactory, even when PA6 weight content is as low as 20. This indicates simplified Palierne's model, i.e., eq. (4) cannot fit well the storage modulus data at low frequency. The interface between PP and PA6 is a

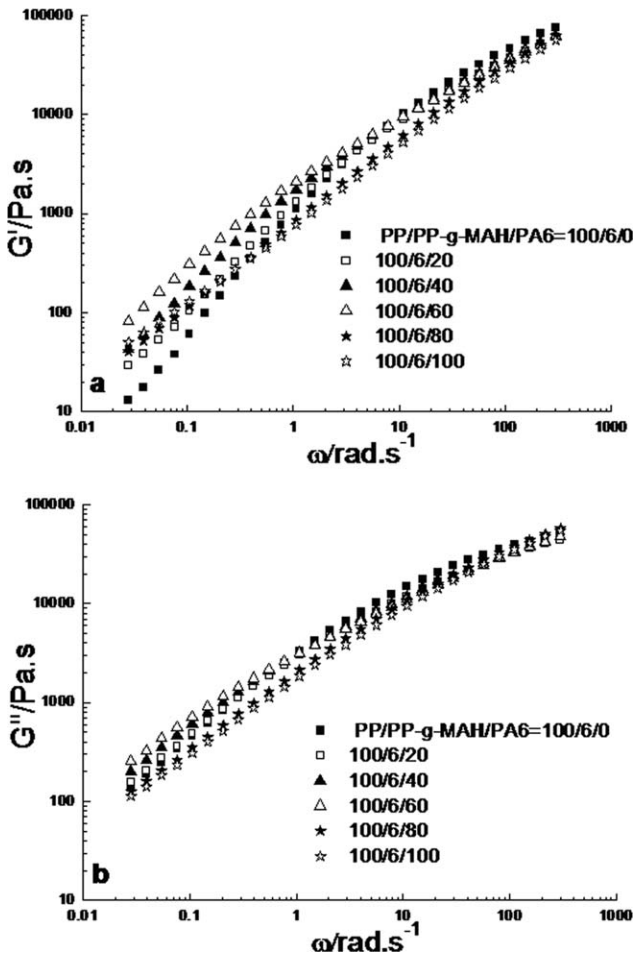

Figure 3. (a) Storage modulus and (b) loss modulus vs. angular frequency of PP/PP-*g*-MAH/PA6 blends at 230°C.

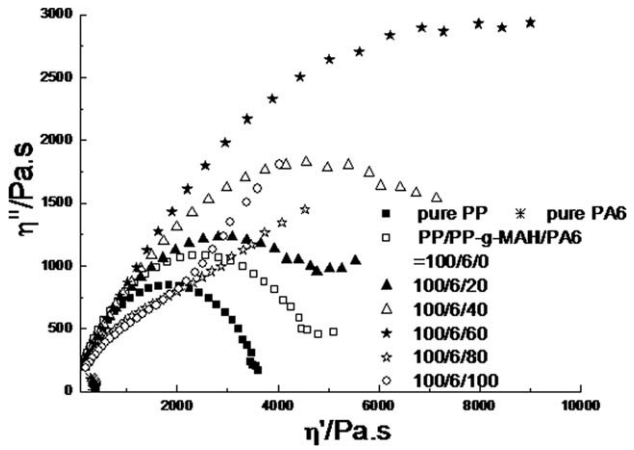

Figure 4. Cole–Cole plots of PP/PP-*g*-MAH/PA6 blends and pure PP and PA6 at 230°C.

reacted copolymer PP-(PP-*g*-MAH)-PA6, formed by the carboxyl group in maleic anhydride of PP-*g*-MAH reacts with the amino end group of PA6. The expanded Palierne's considers the surface dilatation modulus $\beta^*_d(\omega)$ and surface shear modulus $\beta^*_s(\omega)$. In the work of De-an Shi and co-workers,[10] the surface shear modulus is taken into account in the Palierne's model, which is calculated based on the lightly crosslinked rubber model. The surface dilatation modulus is neglected since the change of interfacial area is considered to be very small. Thus in present work, the Palierne's model with α/R and surface shear modulus divided by R (i.e., $\beta^*_s(\omega)/R$) is considered to fit the data. Figure 6 shows the fitting results. This time the Palierne's model [eq. (1)] fits the data well with PA6 weight content of 20, 40, and even 60. And the fitting curve deviate the experimental data at frequency higher than 0.1 rad s^{-1} for PA6 weight content of 80 and 100 because the morphology of the blends is no longer droplet dispersed in matrix. Figure 7 is the fitting curves by Bousmina's model, i.e., eq. (6). For the blend with PA6 weight content of 20, Bousmina's model fits the storage modulus data well. When PA6 content increases from 40 to 60, the deviation between the fitting curve and experimental data increases. For PA6 weight content of 80 and 100, the fitting curves can not overlap the data. By comparison between Figures 5, 6, and 7, one can find the Palierne's model with two parameters α/R and $\beta^*_s(\omega)/R$ is better than Bousmina's model in fitting the experimental storage modulus data, and Bousmina's model is better than the simplified Palierne's model, eq. (4).

The interfacial tension values obtained by fitting the storage modulus data using Palierne's model with two parameters α/R and $\beta^*_s(\omega)/R$ are listed in Table I.

For PP/PP-*g*-MAH /PA6 = 100/6/40 (wt), the average R_v is 0.25 μm, thus the interfacial tension is 0.076 mN/m, $\beta^*_s(\omega)$ =0.064 mN/m. For PP/PP-*g*-MAH/PA6 = 100/6/20 (wt), the average R_v is 0.6 μm (the SEM photo is not shown), thus the interfacial tension is 0.258 mN/m, $\beta^*_s(\omega)$ = 0.077 mN/m. These interfacial tension values are much lower than that of umcompatibilized PP/PA6 blend, for example, 13.61 mN/m for PP/PA6 blend at 230°C.[18] It is clear the interfacial tension between PP/PP-*g*-MAH/PA6 (100/6/40) is lower than that of PP/PP-*g*-MAH/PA6 (100/6/20), which is in accordance with the higher complex viscosity and dynamic modulus of the former than the latter, as shown in Figures 2 and 3.

The prediction on dynamic modulus for usual polymer blends by Bousmina's model is similar to that of Palierne's model. However, the difference between Bousmina's model and Palierne's model is that the former account for the structured materials as mentioned above.[20] Bousmina's model

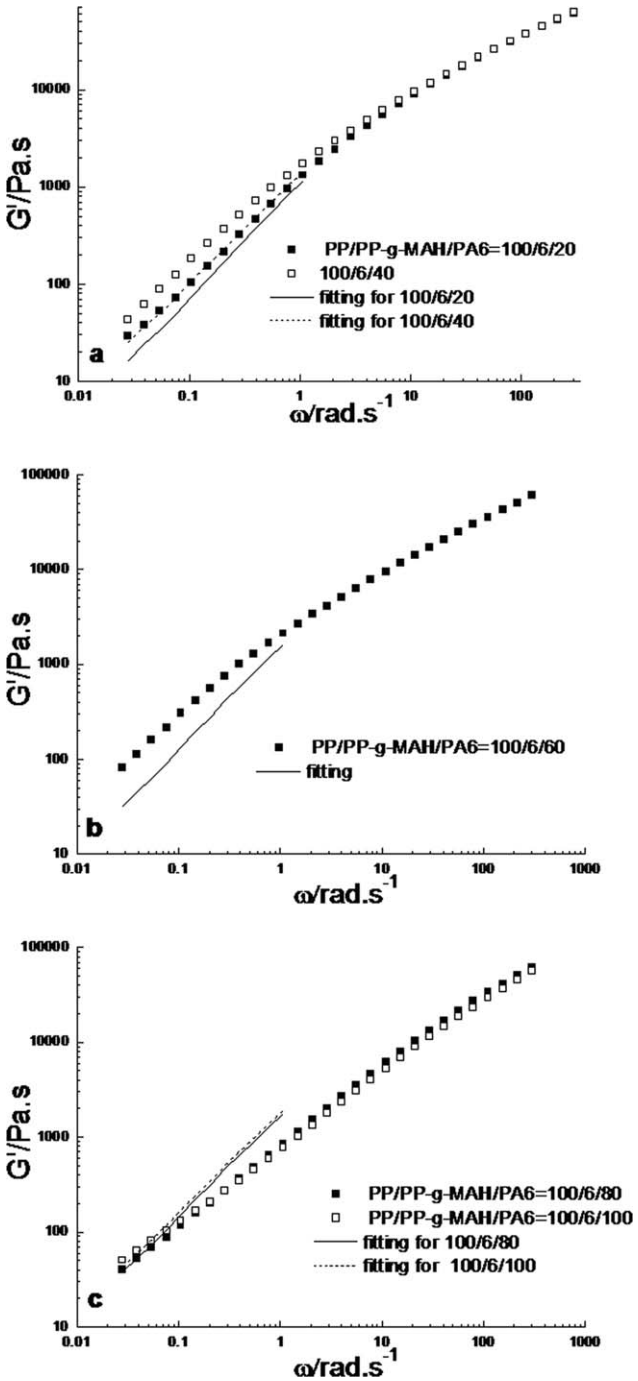

Figure 5. Fit of the dynamic storage modulus data to Palierne's model with α/R for the PP/PP-*g*-MAH/PA6 blends.

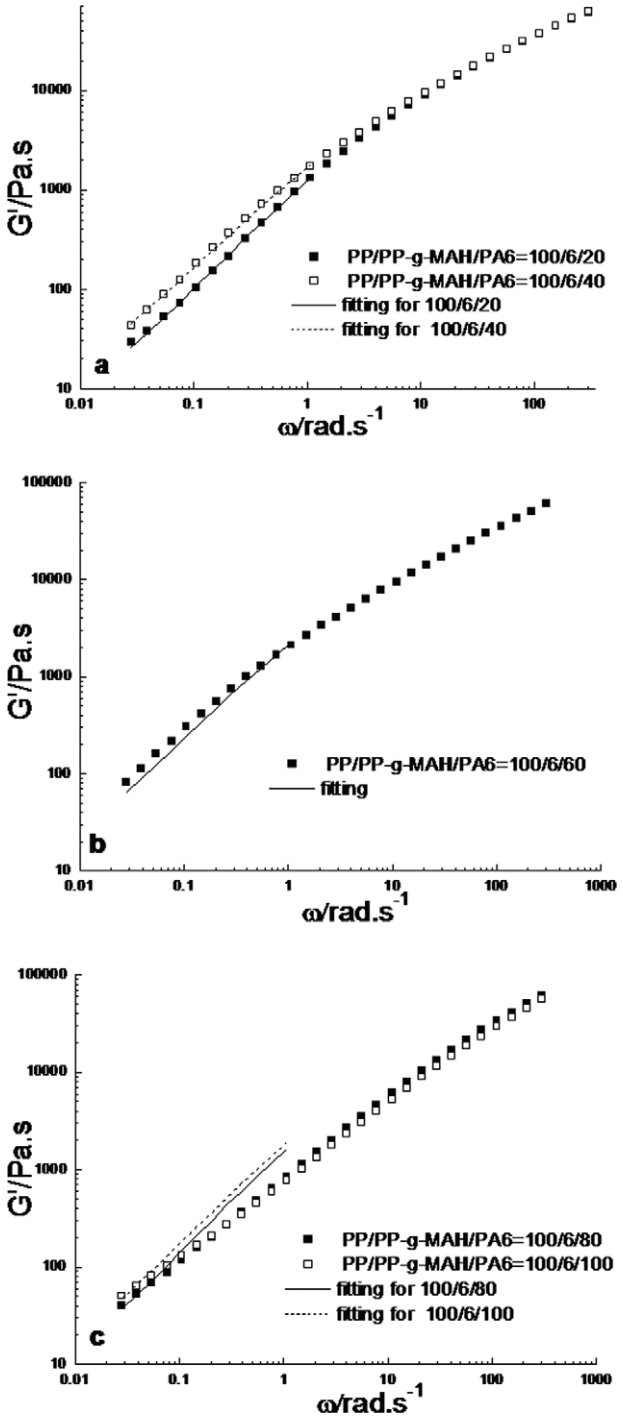

Figure 6. Fit of the dynamic storage modulus data to Palierne's model with α/R and $\beta^*_s(\omega)/R$ for the PP/PP-*g*-MAH/PA6 blends.

considers the blend as a three-region system: spherical droplets surrounded by matrix shells dispersed in a homogeneous matrix. And Bousmina's model considers the flow circulation inside and outside the droplet, hence it corroborate the experimental data of compatibilized blends, although it works out for compatibilized free blends.[20] This explains Bousmina's model is better than Palieren's model with one parameter in our work.

For PP/PA6 blends to which a polypropylene grafted maleic anhydride (PP-*g*-MAH) was added, a reacted copolymer PP-(PP-*g*-MAH)-PA6 interface was formed by the carboxyl group in maleic anhydride of PP-*g*-MAH reacts with the amino end group of PA6. The reacted copolymer PP-(PP-*g*-MAH)-PA6 interface layer presents resistance to shear deformation. The interface has two mechanical properties: the equilibrium interfacial tension and an interfacial dilation modulus/surface shear

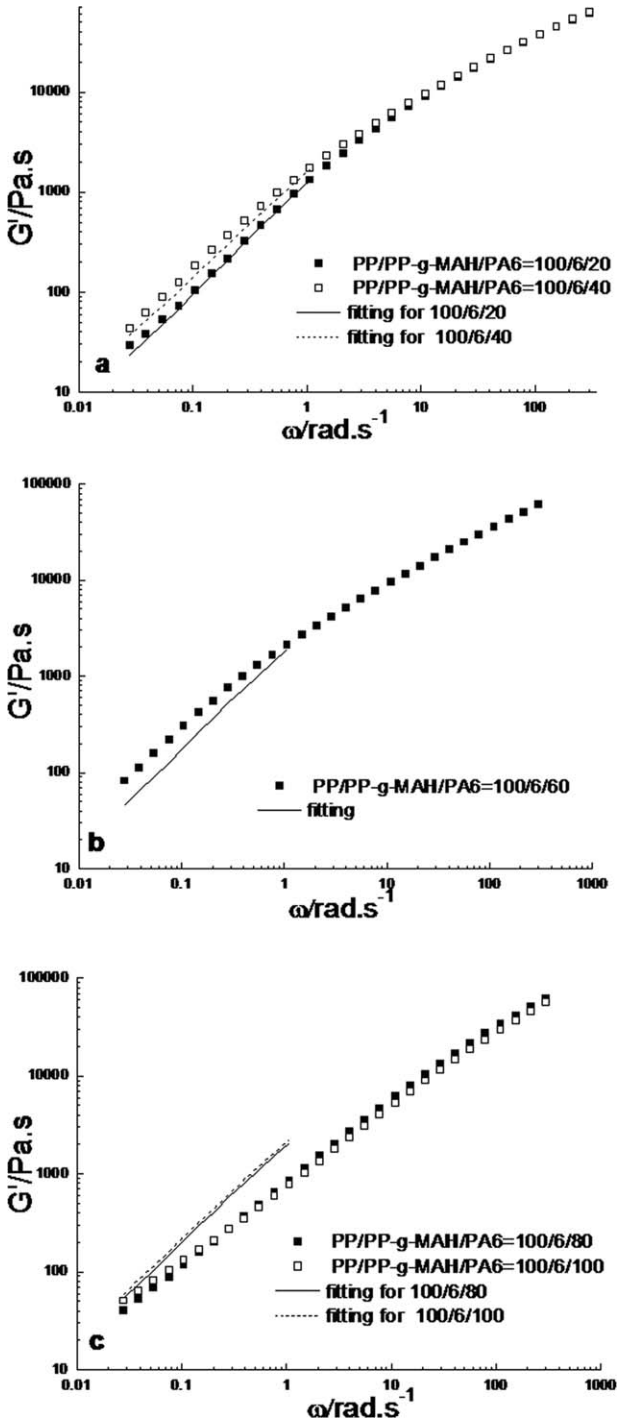

Figure 7. Fit of the dynamic storage modulus data to Bousmina's model for the PP/PP-*g*-MAH/PA6 blends.

Table I. Interfacial Tension and Surface Shear Modulus Divided by R

PP/PP-*g*-MAH/PA6	100/6/20	100/6/40	100/6/60	100/6/80	100/6/100
α/R (N/m^2)	429.39	303.74	393.66	999.9	999.9
$\beta^*_s(\omega)/R$ (N/m^2)	128.53	254.45	337.61	0	0

modulus. The surface shear modulus can be associated with the resistance to shear deformation.[20] Bousmina's model has only one parameter, and it does not include the surface shear modulus. Palierne's model with two parameters considers the surface shear modulus for compatibilized blends, hence it presents a fine fitting result.

Relaxation Time Spectrum of PP/PP-*g*-MAH/PA6 Blending Melts

The weighted relaxation time spectrum of PP/PP-*g*-MAH/PA6 blending melts can be obtained by using the approximation formula of dynamic modulus[16]

$$H(\tau)=G'\left[d\log G'/d\log\omega-\frac{1}{2}(d\log G'/d\log\omega)^2-(1/4.606)d^2\log G'/(d\log\omega)^2\right]_{1/\omega=\tau/\sqrt{2}} \quad (7)$$

The weighted relaxation time spectra of PP/PP-*g*-MAH/PA6 blends at 230°C are calculated using eq. (7), as shown in Figure 8. Similar to the Cole–Cole plots shown in Figure 4, the relaxation spectra curve of PP is a circle arc. The relaxation spectra of the blends with PA6 weight content 0–60 have a main arc and a tail. The main arc corresponds to the relaxation of PP matrix, the tail corresponds to that of PA6 dispersed phase for blends with PA6 weight content 0–60. The relaxation spectra curves of the blends with PA6 weight content 80–100 are different.

The expression for the estimation of the longest form relaxation time τ_p of dispersed phase droplets due to interfacial tension is[7]

$$\tau_p=\frac{R_v\eta_m}{4\alpha}\frac{(19K+16)(2K+3-2\emptyset(K-1))}{10(K+1)-2\emptyset(5K+2)} \quad (8)$$

where $K=\eta_d/\eta_m$. Using eq. (8) and the α/R_v obtained by model fitting which are listed in Table I, the longest form relaxation time can be obtained, which is 12.98, 20.61, and 17.37 s for the blends with PA6 weight content 20, 40, and 60, respectively. The three values are shown in Figure 8.

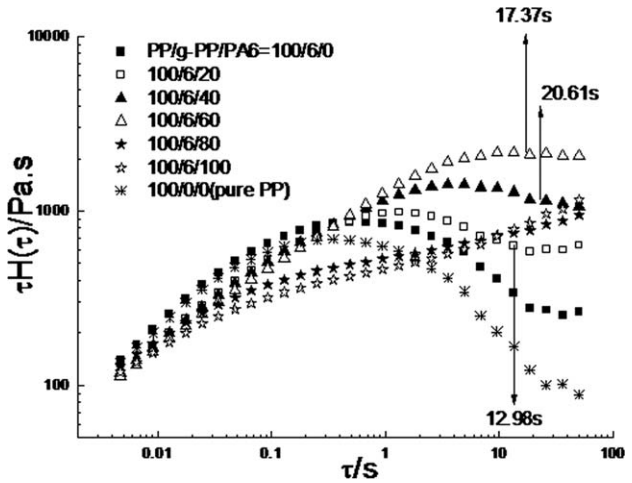

Figure 8. Relaxation time spectra of PP/PP-*g*-MAH/PA6 and pure PP at 230°C.

CONCLUSIONS

SEM micrograph shows that when the weight ratio of PP/PP-*g*-MAH/PA6 is 100/6/40, PA6 phase is the dispersed phase and PP is the matrix. When the weight ratio is 100/6/60, the morphology of the blend is semi-cocontinuous. Coarse PA6 zones which are round or irregular can be observed when the weight ratio is 100/6/80. The dynamic rheological measurement shows that when the weight ratio of PP/PP-*g*-MAH/PA6 increases from 100/6/0 to 100/6/60, the complex viscosity and dynamic modulus at low frequency increase gradually, but when the weight ratio of PP/PP-*g*-MAH/PA6 continues to increase to 100/6/80 and 100/6/100, the complex viscosity and dynamic modulus decrease. Palierne's models and Bousmina's model have been applied to fit the storage modulus data at low frequency. The Palierne's model with only one parameter α/R cannot fit well the data. Bousmina's model can fit the data well when the weight ratio of PP/PP-*g*-MAH/PA6 is 100/6/20 and 100/6/40, respectively. Palierne's model with two parameters α/R and $\beta^*_s(\omega)/R$ can fit the data rather well when the weight ratio of PP/PP-*g*-MAH/PA6 is 100/6/20, 100/6/40, and 100/6/60. The Cole–Cole plots show the blends have a main arc and a tail when the weight ratio of PP/PP-*g*-MAH/PA6 is during 100/6/20–100/6/60, respectively, but the Cole–Cole plots show different shapes when the weight ratio increases to 100/6/80 and 100/6/100. The weighted relaxation spectra of the blends have similar characteristics to the Cole–Cole plots. The reason is possibly the phase inversion occurs when PA6 weight content is close to 50%.

ACKNOWLEDGMENTS

This work was supported by two foundation items: Project (Nos. 201310292051X) by College Students Practice & Innovation Fund of Jiangsu Province, China and Project (No. 201310292003x) by 2013' the Challenge Cup, Outstanding' Innovation Fund of Changzhou University, China.

REFERENCES

1. Shashidhara, G. M.; Biswas, D.; Pai, B. S.; Kadiyala, A. K.; Wasim Feroze, G. S.; Ganesh, M. *Polym. Bull.* **2009**, *63*, 147.

2. Bai, S. L.; Wang, G. T.; Hiver, J. M.; G'Sell, C. *Polymer* **2004**, *45*, 3063.
3. Shokoohi, S.; Arefazar, A.; Naderi, G. *Mater. Des.* **2011**, *32*, 1697.
4. Li, J.; Bao, R. Y.; Yang, W.; Xie, B. H.; Yang, M. B. *Mater. Des.* **2012**, *40*, 392.
5. Darie, R. N.; Brebu, M.; Vasile, C.; Kozlowski, M. *Polym. Degrad. Stabil.* **2003**, *80*, 551.
6. Utracki, L. A. Polymer Alloys and Blends; Carl Hanser: New York, **1989**.
7. Palierne, J. F. *Rheol. Acta* **1990**, *29*, 204.
8. Choi, S. J.; Schowalter, W. R. *Phys. Fluids* **1975**, *18*, 420.
9. Gramespacher, H.; Meissner, J. *J. Rheol.* **1992**, *36*, 1127.
10. Shi, D. A.; Ke, Z.; Yang, J. H.; Gao, Y.; Wu, J.; Yin, J. H. *Macromolecules* **2002**, *35*, 8005.
11. Graebling, D.; Muller, R.; Palierne, J. F. *Macromolecules* **1993**, *26*, 320.
12. Xiang, F. M.; Shi, Y. Y.; Li, X. X.; Huang, T.; Chen, C.; Peng, Y.; Wang, Y. *Eur. Polym. J.* **2012**, *48*, 350.
13. Wu, D. F.; Zhang, Y. S.; Zhang, M.; Zhou, W. D. *Eur. Polym. J.* **2008**, *44*, 2171.
14. Li, L. P.; Yin, B.; Zhou, Y.; Gong, L.; Yang, M. B.; Xie, B. H.; Chen, C. *Polymer* **2012**, *53*, 3043.
15. Larson, R. G. The Structure and Rheology of Complex Fluids; Oxford University Press: New York, **1999**.
16. Tschoegl, N. W. The Phenomenological Theory of Linear Viscoelastic Behavior; Springer: Berlin, **1989**.
17. Macaúbas, P. H. P.; Demarquette, N. R. *Polymer* **2001**, *42*, 2543.
18. Wilkinson, A. N.; Clemens, M. L.; Harding, V. M. *Polymer* **2004**, *45*, 5239.
19. Asthana, H.; Jayaraman, K. *Macromolecules* **1999**, *32*, 3412.
20. Bousmina, M. *Rheol. Acta* **1999**, *38*, 73.
21. Lacroix, C.; Bousmina, M.; Carreau, P. J.; Favis, B. D.; Michel, A. *Polymer* **1996**, *37*, 2939.